RSC Advances

ROYAL SOCIETY OF CHEMISTRY

www.rsc.org/advances

Journal Name

RSCPublishing

ARTICLE

Design of Multifunctional FePt/GO Nanocompsites for Targeting, Dual-Modal Imaging Diagnostic and in situ Therapeutic Potential Theranostic Platform

Cite this: DOI: 10.1039/xoxxooooox

Received ooth January 2012,
Accepted ooth January 2012

DOI: 10.1039/xoxxooooox

www.rsc.org/

Xiuwen Zheng,*[a,b] WeihongChen,[a,b] Ping Cui,[a] ZhimingWang,[a] Wei Zhang,[a,b]

In this work, highly monodispersed chemically disordered face centered cubic (fcc) FePt nanoparticles (NPs) were assembled on graphene oxide (GO) surface to form FePt/GO nanocomposites via a simple polyol protocol. Conjugated with the biocompatible 6-arm polyethylene glycol-amine (PEG) polymer, folic acid (FA) and fluorescein isothiocyanate (FITC), the as-prepared nanocomposites exhibit high stability in physiological solutions, targeted delivery to folate receptor(FR)-positive cancer cells and dual-modal visualization of cellular uptake by fluorescence (FITC) and magnetic resonance imaging (MRI). As a pH-sensitive agent, the fccFePt NPs displays high cytotoxicity because of the generation of highly reactive oxygen species (ROS) within cancer cells. Due to their targeting, diagnostic and therapeutic functions, the FePt/GO nanocomposites are therefore promising for potential theranostic applications in cancer treatment.

1. Introduction

During the past decades, one of the most important emerging multidisciplinary areas in nanotechnology is cancer nanotechnology, which aims to develop effective nanotheranostic agents for the longstanding problems in cancer early diagnosis and therapy.[1-5] In contrast to the separate nanomaterials for therapy and diagnosis, "nanotheranostics" have potential to overcome undesirable difficulties in biodistribution and selectivity that currently exist between distinct imaging and therapeutic agents.[3] The ultimate goal is to gain the desired theranostic agents with the ability of targeting, multimodality imaging diagnosis the diseased tissue and simultaneously treatment with as little as possible side effects.[2,6] Therefore, great progresses have been made for the research of theranostic agents. For example, Ke et al. designed a multifunctional theranostic agent composed of gold-nanoshelled microcapsules (GNS-MCs) and ultrasound-responsive polymeric microcapsules for systemic contrast-enhanced ultrasound imaging diagnosis have been successfully constructed, which hold a great potential for ultrasound-guided photothermal tumor therapy.[7] Gao et al. conjugated Au and □-Fe_2O_3 NPs with RGD and FITC-DEVD to achieve preferential binding to integrin □□□3-rich human liver cancer cells (HepG2), enabling the catalytic formation of hydroxyl radicals (·OH) and real-time monitoring of ·OH-induced caspase-3-dependent apoptosis in these cancer cells.[8] Using a layer-by-layer self-assembly approach, chen et al. prepared a novel class of multifunctional nanocompositeswithsuperparamagnetic iron oxide nanoparticles (IONPs), upconversion nanoparticles (UCNPs), gold shell for in vitro targeted upconversion luminescence (UCL), magnetic resonance (MR), and dark-field scattering multimodal imaging of cells.[9] The NIR optical absorption offered by the gold shell also enables molecular and magnetic dual-targeted photothermal destruction of cancer cells. And also, hexagonal phase $NaYF_4$:Yb,Er/$NaGdF_4$ core-shell UCNPs conjugated with Ce6, a photodynamic therapy (PDT) drug, have been successfully prepared and used not only as dual-modal imaging probes for accurate diagnosis but also as PDT agents for efficient therapy.[10] All of aforementioned works present a unique strategy for multi-modal imaging guided, magnetically targeted physical cancer therapy and highlights the promise of using multifunctional nanostructures for novel cancer theranostics.

Recently, monodispersiveFePt NPs have attracted considerable attention due to their fascinating potential applications in biomedical sciences of CT/MRI molecular imaging contrast agent,[11,12] drug delivery,[13,14] biosensing,[15] etc. And also, some exciting results have been reported that the FePt NPs have potential therapeutic functions for cancer therapy as the chemotherapeutic agents[16] or hyperthermia agents[17,18] due to the release of Fe or the photothermal and magnetic-thermal effects activated by the near infrared (NIR) femtosecond laser or external magnetic fields, respectively. Thus, FePt-based nanocomposites present an opportunity in realizing CT, MRI, magnetic-thermal, photothermal treatments all within a single agent, and will open up a new strategy to develop new anticancer nanomedicine agents with both diagnostic and therapeutic functions.

As well known, GO can be functionalized by biocompatible polymers such as PEG, to acquire improved stability in physiological environments. Functionalized nanoscale GO bioconjugates have been widely explored as drug and gene carriers.[19,20] Here, combined the merits of FePt (pH-responsive FePt "chemotherapy") and GO (functionalize by biocompatible polymers), we aim to design a new class of theranostic agent

with targeting, imaging and therapeutic functions. FePt/GO nanocomposites were synthesized by a simple polycol route and then functionalized with the biocompatible polyethylene glycol (PEG) polymer. Folic acid (FA) and fluorescein isothiocyanate (FITC) were conjugated onto the as-prepared FePt/GO-PEG nanocomposites for the effective targeting of folate receptor-rich tumor cells and the dual-modal visualization of cellular uptake by fluorescence (FITC) and magnetic resonance imaging. After the cell uptake, the fccFePt nanoparticles (NPs) displays high cytotoxicity due to the generation of ROS within cells. Due to the targeting, diagnostic and therapeutic functions, the carbon-based FePtnanocomposites are therefore promising for future nanotheranostic applications in cancer treatment.

2.Experimental section

2.1Materials

General: Analytical reagents, such as $FeCl_2{\cdot}4H_2O$, $H_2PtCl_6{\cdot}6H_2O$, NaOH, N-hydroxysuccinimide (NHS), folate acid (FA), fluorescein isothiocyanate (FITC), 1-(3-dimethylaminopropyl)-3-ethylcarbodiimide (EDC), tetraethylene glycol, were all purchased from J&K Chemical Ltd. Spin Column was purchased from Beyotime Institute of Biotechnology. 6-arm-polyethylene glycol-amine (10 kDa) was purchased from SunBio, Inc. The single layer graphene oxide (GO) was made by a modified Hummers method starting from graphite[21].

2.2 Synthesis of FePt/GO nanocomposites

The FePt/GO nanocomposites were synthesized as in our previously reported route with a slight modification.[22] In a typical synthesis, GO (20 mg) were completely dispersed into tetraethylene glycol with the assistance of sonication. After that, $FeCl_2{\cdot}4H_2O$ (0.15 g, 0.75 mmol) and $H_2PtCl_6{\cdot}6H_2O$ dispersed in tetraethylene glycol solution (10 mL, 3.86×10^{-5} mol mL^{-1}) and NaOH (0.15 g, 3.175 mmol) were added into the solution under sonication. The mixed solutions were heated up to ca. 260°C and kept at this temperature for 1 h under a nitrogen atmosphere. The products were collected by centrifugation, rinsed several times with deionized water. The final products were dispersed into PBS (pH = 7, ca. 5 mg mL^{-1}) solution.

2.3 Surface modification of FePt/GO NPs with amined PEG

Briefly, 100 mg of 6-Arm polyethylene glycol-amine, 200 mg EDC and 100 mg NHS were added into FePt/GO solutions (50 mL, 5 mg mL^{-1}) and ultrasonicated for 10 min. The reaction solution was stirred overnight at room temperature. The resulting product was purified by centrifugation at 12 000 r/min for 20 min and washed three times with D.I. water to remove unreacted PEG and other reagents.

2.4 Conjugation of FA and FITC onto FePt/GO-PEG NPs

FA (30 mg) and FITC (20 mg, dissolved in DMSO, 2 mg mL^{-1}) were added into FePt/GO-PEG PBS solutions (10 mL, 2 mg mL^{-1}) with the assistance of sonication for 30 min. After that, 200 mg of EDC and 100 mg of NHS were added to the solution. The solution was stirred overnight at room temperature. The resulting product were purified by centrifugation at 12 000 r/min for 20 min and washed several times with D.I. water to remove unreacted FA, FITC, and other reagents. The obtained products were denoted as FePt/GO-PEG-FA-FITC. The final products were redispersed into D.I. water for further application. The final concentrations (Fe content) are 661.7 μg mL^{-1} by inductively coupled plasma (ICP) measurement.

2.5 Cell line and cell culture

The MCF-7 and A549 cell line was kindly provided by Professor Haiyan Liu, Soochow University. Cells were cultured in DMEM medium with 10% fetal bovine serum and incubated in a humidified atmosphere at 37°C with 5% CO_2.

2.6 Confocal imaging of cells

The as-prepared FePt/GO-PEG-FA-FITC NPs (20 μg mL^{-1} for Fe concentration) were incubated with MCF-7 and A549 cells in 24-well plates for 12 h at 37 °C, respectively. Finally, fluorescence microscopy images were captured by a laser confocal microscope.

2.7 Characterization of reactive oxygen species (ROS) formation in vitro

The MCF-7 cells were seeded in 6-well microplates and incubated for 20 min with the DCFH-DA, and then, washed with fresh DMEM medium supplemented with 10% fetal bovine serum for three times and treated with the FePt/GO-PEG-FA-FITC composites at a final Fe concentration of 20 μg mL^{-1}, 60 μg mL^{-1}, and 100 μg mL^{-1}, respectively. After 6 h of cells-NPs incubation, the MCF-7 cells were characterized by fluorescence spectrophotometer (excited at 488 nm). Data were expressed as mean ± SD. Differences in ROS generation between cells treated with NPs and controls were considered statistically significant performing a t-student test with a p-value<0.05.

2.8 Effect of the NPs on chromosomal DNA fragmentation

The effect of the NPs on chromosomal DNA fragmentation was performed by DNA Ladder Extraction Kit with Spin Column. First, the MCF-7 cells were seeded in cell culture dishes and incubated for 24 h with the FePt/GO-PEG-FA-FITC composites at a final Fe concentration of 20 μg mL-1, 60 μg mL^{-1}, and 100 μg mL^{-1}, then, washed with fresh DMEM medium supplemented without 10% fetal bovine serum for three times, the MCF-7 cells were collected into 1.5 mL centrifuge tube for DNA ladder extraction. DNA fragments obtained by this method were loaded onto a 1.5% (w/v) agarose horizontal gel. Agarose gel electrophoresis (AGE) was performed in TBE buffer (pH 8.0) at 15 V cm^{-1}. The gel was visualized by staining with ethidium bromide and photographed. DNA standard mark DL2000 (Takara Biotechnology CO., LTD) was used as a DNA size marker.

2.9 In vitro cytotoxicity assay

WST assay was performed to evaluate the cytotoxicity of FePt/GO-PEG-FA-FITC composites. The MCF-7 cells were seeded in 96-well plates at a density of 1×10^4 cells in 100 μL culture medium and maintained for 24 h. Then, cells were incubated for 24 h with the FePt/GO-PEG-FA-FITC composites at different Fe concentration of 1 μg mL^{-1}, 5 μg mL^{-1}, 15 μg mL^{-1}, 50 μg mL^{-1}, 75 μg mL^{-1}, and 100 μg mL^{-1} respectively, then washed with PBS buffer for three times and added fresh DMEM medium supplemented with 10% fetal bovine serum. The relative cellular viability was examined by the WST assay. The data were presented as mean ± SD.

2.10 Prussian blue staining of cells

The MCF-7 cells were seeded in 96-well plates then incubated with 20 μg mL^{-1}FePt/GO-PEG-FA-FITC for 24 h, respectively. The cells were then fixed with 4% paraformaldehyde for 15 min and incubated with Pearls reagent (4% potassium ferrocyanide and 12% HCl, 50:50 vol vol^{-1}) for 30 min at room temperature under agitation. The cells were then rinsed well with PBS.

2.11 Ultrathin sections of cells

The MCF-7 cells were seeded in 6-well plates. The cells were then treated with 20 μg mL^{-1}FePt/GO-PEG-FA-FITC for 10 h. The cells were collected via trypsin treatment and pelleted at 3 500 rpm for 15 min. The pellets were fixed using 4% paraformaldehyde and routinely processed for ultrathin

sectioning. The ultrathin sections were prepared using an ultramicrotome, routinely stained with uranyl acetate and lead citrate, and examined on a transmission electron microscope (TEM).

2.12 In vitro MR imaging

The minimum detectable iron concentration was obtained by incubation of separate batches of cells (5×10^5 cells mL^{-1}) at different iron concentration of 5, 10, 15, and 20 μg mL^{-1} for 24 h, respectively. Imaging parameters of T2-weighted images (T2WI) by multi slice multi echo (MSME) experiments on 11.7 T Bruker micro 2.5 micro-MRI system with repetition time (TR) = 5000 ms, echo time (TE) = 80 ms, imaging matrix = 128 × 128, slice thickness = 1 mm, and file of vision (FOV) = 2.5 cm × 2.5 cm.

2.13 Instrumentation.

The morphology and composition of NPs were characterized by transmission electron microscopy (TEM) (JEM-2100, JEOL, Japan) equipped with an Energy Dispersive Spectrometer. Magnetic measurement was carried out at room temperature on a Magnetic Property Measurement System (MPMS) (SQUID VSM, Quantum Design, USA). Ultraviolet and visible spectra were obtained on UV-Vis spectrometer (Cary 60, Agilent, USA). The iron concentration was measured using Inductively Coupled Plasma Optical Emission Spectrometer (ICP-OES VISTA-MPX, Varian, USA). WST assay was performed with Microplate Reader (Eon, Biotek, USA). Cell lines were cultured in a water-jacketed CO2 incubator (3111, Thermo, USA). The MRI was carried out on an 11.7 T micro 2.5 micro-MRI system (Avance 500WB, Bruker, Germany) with a conventional spin echo acquisition. Relaxivity (r2) with unit $mM^{-1}s^{-1}$ was calculated through the curve-fitting of the reciprocal of the relaxation time versus the iron concentration (mM Fe). Cell slices were obtained by a cell slicing machine (EMUC6, Leica, Germany). Fluorescence microscopy images were captured by a laser confocal microscope (CS SP8, Leica, Germany).

3. Results and Discussions

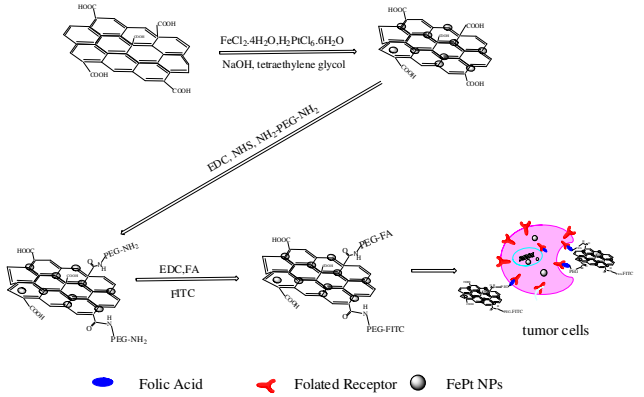

Sheme 1. A schematic illustration of FePt/GO-PEG-FA-FITCnanocomposite synthesis.

Using the pretreated GO (Figure S1), carbon-based FePt nanocomposites were successfully synthesized via our reported methods with moderate modification. Ultrasmall fcc FePt NPs are assembled on the GO surface to form FePt/GO nanocomposites. This strategy is schematically illustrated in Scheme 1. First, FePt/GO nanocomposites were synthesized via the simple polyol protocol. Next, the nanocomposites were covalently conjugated with the polyethylene glycol (PEG) polymer via the EDC/NHS chemistry to endow the NPs with good biocompatibility and physiological stability. At last, folic acid (FA) and fluorescein isothiocyanate (FITC) was covalently binded to the PEG modified NPs, thus allowing it to specifically target FA receptor-rich cancer cells and capability of simultaneously performing dual-modality imaging by fluorescence and magnetic resonance.

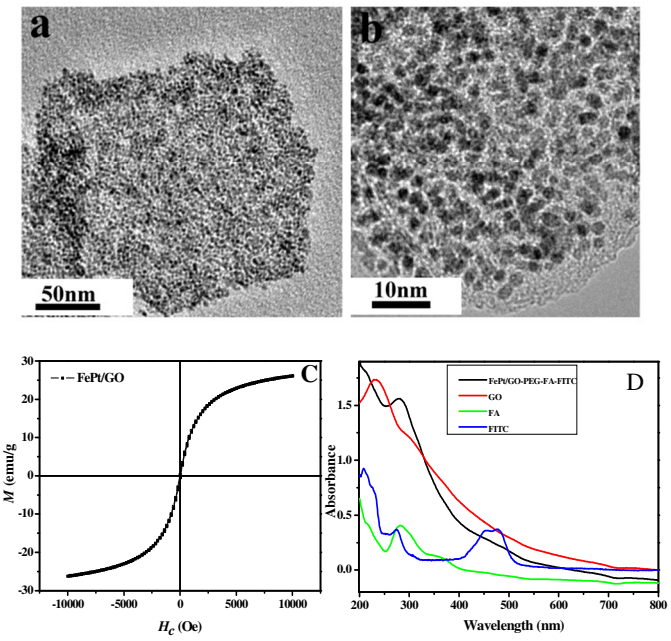

Figure 1.(a,b)TEM images of as-prepared FePt/GO-PEG NPs with different magnification, (c)Magnetization curves of as-prepared FePt/GO NPs.(d) UV/Vis spectra of the FePt/GO-PEG-FA-FITC NPs, GO, FA and FITC in aqueous solution.

Figure 1a and b are the typical TEM images for the as-prepared FePt/GO nanocompoistes with different magnification, showing the uniformly distribution of FePt NPs on GO surface. More importantly, few aggregations of FePt NPs were found in solution, which indicates the high selective nucleation of FePt NPs on the functional GO surface. The average diameters for FePt NPs were *ca.* 2-3 nm. The EDX analysis of the samples revealed that the alloying compositions of the three samples were $Fe_{58}Pt_{42}$. The ICP analysis of these samples revealed their final particle composition to be $Fe_{57}Pt_{43}$, which are consistent with the EDX measurement. The magnetic properties of the as-prepared FePt/GO were measured by the field-dependent magnetization measurement. The magnetic hysteresis loops (Figure 1c) showed that the samples exhibited superparamagneticbehaviorat 300 K. The saturated mass magnetizations (Ms) at 300 K are 26.15 emu g^{-1}. 6-arm-polyethylene glycol-amine was then covalently conjugated to the FePt/GO to endow the NPs with good biocompatibility and physiological stability. Conjugation of FA and FITC to FePt/GO-PEG through formation of an amide bond by the

reaction between the COOH groups of FA and NH_2 groups of FePt/GO-PEG and formation of thiourea bond by NCS groups of FITC and NH_2 groups of FePt/GO-PEG) was confirmed by UV/Vis and fluorescence measurements. In the UV/Vis spectra (Figure 1d) for FePt/GO-PEG-FA-FITC, the peak at 230 nm for characteristic of GO disappears while a new peak at 278 nm appears due to the presence of FA and FITC in the FePt/GO. Fuorescence peak of the FePt/GO-PEG-FA-FITC appears at 518 nm with excitation wavelength of 488 nm, which is consistent with that of the free FITC, confirming successful conjugation of FITC on the surface of the FePt/GO NPs. These FePt/GO-PEG-FA-FITC nanocomposites exhibited excellent stability in DMEM medium with 10% fetal bovine serum for two months without precipitation (Figure S2). To elucidate this stability of the NPs in DMEM medium with 10% fetal bovine serum, the zeta potentials of the FePt/GO-PEG-FA-FITC NPs in water and in DMEM medium with 10% fetal bovine serum were measured to be -45.9 mV and -15.0 mV, respectively. Clearly, the great difference in the surface charges of the magnetic NPs is due to the zeta potentials of the DMEM medium with 10% fetal bovine serum without NPs (-13.7 mV), but we still see that the FePt/GO-PEG-FA-FITC NPs in water (-45.9 mV) is lower than the -30 mV, which means that stability of the NPs.

To check the targeting function of the conjugated FA, the complex FePt/GO-PEG-FA-FITC NPs were incubated with MCF-7 cells (FA receptor positive) and A549 cells (FA receptor negative). The cells were the imaged by confocal fluorescence microscopy (Figure 2a). Much stronger fluorescence was observed in MCF-7 cells than in A549 cells for these two samples, indicating higher uptake of FePt/GO-PEG-FA-FITC for MCF-7 cells. This result further demonstrates the high specific FR targeting of FePt/GO-PEG-FA-FITC. Not only the conjugated FITC could be used in fluorescence visualization imaging modalities, but also the attached superparamagnetic FePt NPs are potential excellent contrast agent for T2-weighted MR images according to the reported literatures.[11,12] After incubation with the FePt/GO-PEG-FA-FITC NPs, MCF-7 cells were transferred into agarose gel pellets and imaged by the 11.7 T Bruker micro scanners. As expected, the NPs labeled MCF-7 (Figure 2b) showed relaxation rate enhancement, depending on the dose. In our study, the imaging contrast for cells incubated with the FePt/GO-PEG-FA-FITC NPs at the Fe concentration of 10μg mL^{-1} is obviously darker than that in case of without NPs. With the increase of concentration, the growth rate of the MR relaxation rate started to decline, the decrease of growth rate is due to cell apoptosis and cytotoxicity impairment when cells incubated with the heavily-labeled NPs (apoptotic cells can be easily washed). These results indicate the great potential for the as-prepared FePt/GO-PEG-FA-FITC for dual-modal imaging contrast for diagnostic functions. WST cell viability assay was performed to evaluate the cytotoxicity of FePt/GO-PEG-FA-FITC composites to FA receptor- positive MCF-7 cells (Figure 3a). Experimental data confirmed that the cytotoxicity was dependent on the Fe concentration. The half-maximum inhibitory concentration (IC50) values are 49.65 μg mL^{-1} for FePt/GO-PEG-FA-FITC. Based on Figure 2-3, one could find that the as-prepared carbon-based nanocomposites exhibit not only dual-modal visualization of cellular uptake by fluorescence and MRI but also potential therapeutic function for FA receptor-positive cancer cells. In our study, MR relaxation rate (1/T2) of MCF-7 cells incubated with the FePt/GO-PEG-FA-FITCNPs composites at different concentrations for 24 h is still very high (12.7 mM^{-1} s^{-1}).

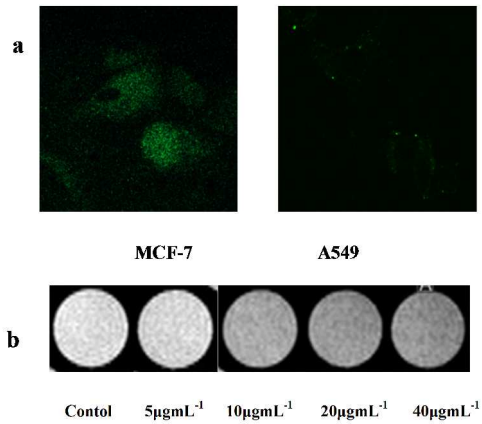

Figure 2.(a) Fluorescence images ofMCF-7 and A549 cellsincubated with the FePt/GO-PEG-FA-FITC NPs, (b)T2 weighted MR images: MCF-7 cells (2×10^5 cells mL^{-1}) incubated with FePt/GO-PEG-FA-FITC NPsat different Fe concentrations for 24 h. The imaging parameters with 11.7 T magnet system: TR = 5000 ms,TE = 80 ms, imaging matrix =128×128, slice thickness = 1 mm, FOV = 2.5 cm*2.5 cm.

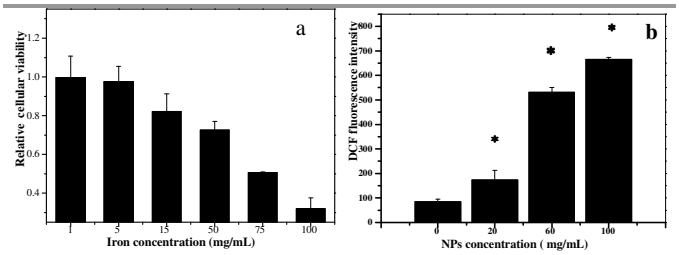

Figure 3. (a)Relative viability of cells incubated with FePt/GO-PEG NPs at different concentrations for 24 h. Error bars were based on quartet samples. (b) Effect of FePt/GO-PEG NPs on intracellular ROS levels in MCF-7 cells after 6 h (n=3). Error bars were based on quartet samples. The asterisks indicate $P < 0.05$.

It 1is well known that the uptake of Fe NPs in cellular system will lead to the Fe buildup and the production of ROS. These effects will induce apoptosis and inflammation,[8,16,23,24] affect the actin cytoskeleton, damage DNA, proteins[25] and eventually cell death. According to the reported results, it is believed that Iron ions released after the degradation of NPs into the acidic endolysosomal compartments could react with hydrogen peroxide produced by the mitochondria, producing highly reactive hydroxyl radicals and ferric ions (Fe^{3+}) through the Fenton reaction.[16,26,27] Here, the assessment of NPs to induce the production of intracellular oxidants was characterized by DCF fluorescence as a reporter of ROS generation. The MCF-7 cells were firstly incubated with DCFH-DA for 20 min, and then, treated with the FePt/GO-

PEG-FA-FITC at a final Fe concentration of 20 μg mL^{-1}, 60 μg mL^{-1}, and 100 μg mL^{-1}, respectively. Following cellular uptake, the DCFH is deprotonated and converted to quinone-like DCF at the presence of ROS. After 6 h of cells-NPs interaction, the MCF-7 cells were tested by fluorescence spectrophotometer (excited at 488 nm), as shown at figure 3b and figure S3. The higher NPs concentration (100 μg mL^{-1}), the higher fluoresces intensity.The obvious toxicity was found at Fe concentration of 50 μg mL^{-1} and 100 μg mL^{-1}, which consistent with the ROS results.

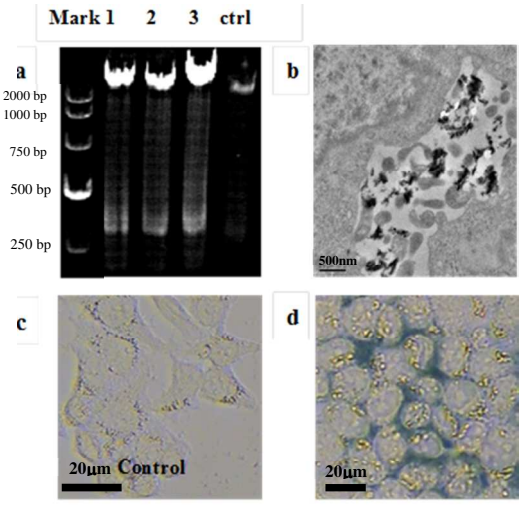

Figure 4. (a) Effect of the NPs on chromosomal DNA fragmentation DL 2000 DNA mark：2000bp；1000bp；750bp；500bp；250bp. Lane1、Lane2 and Lane3：DNA ladder of the cells incubated for 24 h with the FePt/GO-PEG NPs. (b) TEM images of cells exposed to FePt/GO-PEG-FA-FITC, (c,d) Photomicrographs of Prussian blue staining of MCF-7 cells: unlabeled cells as a control, cells incubated with the FePt/GO-PEG NPs at iron concentration of 20 μgmL^{-1} for 24 h.

In order to further test the impact of this nanocomposite on DNA, we performed the DNA Ladder Extraction assay of cell apoptosis. The genotoxicity about DNA results were in good agreement with the cytotoxicity data: the higher the Fe concentration, the more significant damage of DNA in terms of DNA fragmentation length and DNA fragmentation percentage (Figure 4a). This modality of DNA fragmentation is typical of ROS-induced cell death, i.e., giant DNA fragmentation followed by smaller internucleosomal DNA fragmentation shown as a ladder-like pattern.[28,29] These data suggest that the NPs induced DNA fragmentation in an ROS-dependent manner. An ultrastructural examination of the cells treated with FePt/GO-PEG-FA-FITC NPs was performed to confirm that the NPs had interacted with the cells. Obviously, the individual FePt/GO-PEG-FA-FITC NPs with the diameters of 200 nm by TEM were observed in ultrathin sections (Figure 4b). Visible morphological damage was observed for the MCF-7 cells treated with the NPs. A few endoplasmic reticulum and small Golgi complex were damaged by the NPs as observed by the TEM. Many endosomes and lysosomes were observed which demonstrated the toxicity of these NPs. Iron inside the cells was visualized by Prussian Blue staining, a standard protocol widely used to examine cellular uptake of iron oxide NPs.[30] We found that the FePt/GO-PEG-FA-FITC NPs labeled cells are efficient labeled at nearly 90% efficiency (Figure 4c,d). The labeled cells showed clusters of dense blue granules in the cytoplasm, which indicates the location of the NPs.

Conclusions

In this work, we have developed a simple strategy for the preparation of FeP/GO nanocomposites as a therapeutic nanoplatform that combines efficient targeting, dual-modal imaging and therapeutic properties. The conjugation of biocompatible polyethylene glycol, folic acid (FA) and fluorescein isothiocyanate (FITC) endow the as-prepared carbon-based nanocomposites high stability in physiological solutions, targeted delivery to folate receptor-rich cancer cells and dual-modal visualization by fluorescence (FITC) and magnetic resonance imaging. The dual-modal optical/MRI imaging combines the advantages of each single imaging mode to enhance the sensitivity and tissue penetration. After targeting uptake with MCF-7 cells, the as-prepared FePt/GO NPs selectively initiated catalytic formation of ROS, which are toxic to tumor cells. The uptake of Fe into cells and the cytotoxicity mechanism were further characterized by prussian blue staining, ultrastructural examination and the DNA Ladder Extraction. The as-prepared FePt/GO NPs could in principle be coated and conjugated with various kinds of lipid molecules, peptides and antibodies that are specific for different cancer cells. Therefore, the carbon-based FePt NPs are promising for many applications in biomedicine, including multimodality imaging, cell tracking and imaging-guided novel targeted cancer therapies. Further works are ongoing.

Acknowledgements

Financial support of this work by Natural Science Foundation of China (No. 21101087, 21375057, 21205057, 21405074) and Shandong Province Natural Science Foundation (No. ZR2013BL007) are gratefully acknowledged.es.

Notes and references

[a]School of Chemistry & Chemical Engineering, Linyi University,
[b]Shandong provincial Key Laboratory of Detection Technology for Tumor Makers, Linyi University
* Corresponding author E-mail: xwzheng1976@gmail.com

Electronic Supplementary Information (ESI) available: AFM image for GO, TEM image for FePt/CNTs, etc. See DOI: 10.1039/b000000x/

1 C.Li, Nat. Mater. 2014, **13**,110-115.
2 P.Prabhu, V.Patravale, J.Biomed. Nanotechnol. 2012, **8**, 859-882.
3 S.S.Kelkar, T.M.Reineke, Bioconjugate Chem. 2011, **22**, 1879-1903.
4 N.Ahmed, H.Fessi, A.Elaissari, Drug Discovery Today, 2012, **17**, 928-934.
5D.Yoo, J.H.Lee, T.H.Shin, J. Cheon, Acc. Chem. Res. 2011, **44**, 863-874.
6 K.Yang, L.Z.Feng, X.Z.Shi, Z.Liu, Chem.Soc.Rev. 2013, **42**, 530-547.
7 H.T.Ke, J.R.Wang, Z.F.Dai, Y.S. Jin, E.Z.Qu, Z.W.Xing, C.X.Guo, X.L. Yue, J.B.Liu, Angew. Chem. Int. Ed. 2011, **50**, 3017-3021.

8 W.Gao, L.F.Ji, L.Li, G.W.Cui, K.H.Xu, P.Li, B.Tang, Biomaterials, 2012,**33**, 3710-3718.
9 L.Cheng，K.Yang，Y.G.Li, J.H.Chen, C.Wang, M.W.Shao, S.T.Lee, Z.Liu, Angew.Chem.Int.Ed. 2011, **50**, 7385-7390.
10Y.Park, H.M.Kim, J.H.Kim, K.C.Moon, B.Yoo, K.T.Lee, N.Lee, Y.Choi, W.Park, D.S.Ling, K.Na, W.K.Moon, S.H.Choi, H.S. Park, S.Y.Yoon, Y.D.Suh, S.H.Lee, T. Hyeon, Adv. Mater. 2012, **24**, 5755-5761.
11S.Chen, L.J.Wang, S.L.Duce, S.Brown, S. Lee, A.Melzer, S.A.Cuschieri, P.Andre, J. Am. Chem. Soc. 2010, **132**, 15022-15029.
12S.W.Chou, Y.H.Shau, P.C.Wu, Y.S.Yang, D.B.Shieh, C.C.Chen, J. Am. Chem. Soc. 2010, **132**, 13270-13278.
13 T.Fuchigami, R.Kawamura, Y.Kitamoto, M.Nakagawa, Y. Namiki, Biomaterials, 2012, **33**, 1682-1687.
14 Y.M.Liu, K.Yang, L.Chen, J.Zhu, X.X.Ma, H.Xu, Y.G. Li, L.Guo, H. W.Gu, Z.Liu, Nanomed-Nanotechnol. 2013, **9**, 1077-1088.
15 N.Moghimi, K.T.Leung, Anal. Chem. 2013, **85**, 5974–5980.
16 C.J.Xu, Z.L.Yuan, N. Kohler, J.M.Kim, M.A.Chung, S.H.Sun, J. Am. Chem. Soc. 2009, **131**, 15346-15351.
17 S.Maenosono, S. Saita, IEEE Transactions on Magnetics, 2006, **42**, 1638-1642.
18 C.L.Chen, L.R.Kuo, S.Y.Lee, Y.K.Hwu, S.W. Chou, C.C. Chen, F.H. Chang, K.H.Lin, D.H.Tsai, Y.Y.Chen, Biomaterials, 2013, **34**, 1128-1134.
19 K.Yang, L.Z.Feng, X.Z. Shi, Z.Liu, Chem. Soc. Rev. 2013, **142**, 530-547.
20 K. Yang, L.Z. Feng, H. Hong, W.B. Cai, Z. Liu, Nat. Protoc. 2013, 8, 2391-2403.
21 L.M. Zhang, J.G. Xia, Q.H.Zhao, L.W. Liu, Z.J. Zhang, Small. 2010, **6**, 537-544.
22 Q.T. Hu, Z.B. Gan, X.W. Zheng, A.H. Zhao, X. Zhang, J. Nanopart. Res. 2011,**13**, 3191–3197.
23 M. A. Malvindi, V. De Matteis, A. Galeone, V. Brunetti, G. C. Anyfantis, A. Athanassiou, R. Cingolani, P. P.Pompa, PLoS ONE 2014, **9**, e85835.
24 A.Laskar, M.Ghosh, S. I.Khattak, W.Li, X.-M.Yuan, Nanomedicine, 2012, **7**, 705-717.
25 N.Singh, G. J. S.Jenkins, B. C. Nelson, B. J. Marquis, T. G. G. Maffeis, A. P. Brown, P. M. Williams, C. J.Wright, S. H. Doak, Biomaterials 2012, **33**, 163-170.
26 M.Levy, F. Lagarde, V. A.Maraloiu, M. G.Blanchin, F.Gendron, C. Wilhelm, F.Gazeau, Nanotechnol. 2010, **21**, 395103.
27 S. J. H. Soenen, U. Himmelreich, N. Nuytten, M. De Cuyper, Biomaterials 2011, **32**, 195-205.
28 K.Takaki, Y.Higuchi, M.Hashii, C.Ogino, N.Shimizu, J. Biosci. Bioeng. 2014, **117**, 129-133.
29 Y. Higuchi, Biochem. Pharmacol. 2003, **66**, 1527-1535.
30 A. S.Arbab, L. A. Bashaw, B. R. Miller, E. K.Jordan, B. K.Lewis, H. Kalish, J. A.Frank, Radiology 2003, **229**, 838-846.
31 Z.Liu, X.J. Liang, Theranostics 2012, **2**, 235-237.

